Computers and Electronics in Agriculture 137 (2017) 29–40

Contents lists available at ScienceDirect

Computers and Electronics in Agriculture

journal homepage: www.elsevier.com/locate/compag

A pragmatic, automated approach for retroactive calibration of soil moisture sensors using a two-step, soil-specific correction

Caley K. Gasch [a,*], David J. Brown [b], Erin S. Brooks [c], Matt Yourek [c], Matteo Poggio [b], Douglas R. Cobos [b,d], Colin S. Campbell [b,d]

[a] Department of Soil Science, North Dakota State University, PO Box 6050, Fargo, ND 58108-6050, USA
[b] Department of Crop and Soil Sciences, Washington State University, PO Box 646420, Pullman, WA 99164-6420, USA
[c] Department of Biological and Agricultural Engineering, University of Idaho, 875 Perimeter Drive MS 0904, Moscow, ID 83844-0904, USA
[d] METER Group, Inc., 2365 NE Hopkins Ct, Pullman, WA 99163, USA

ARTICLE INFO

Article history:
Received 22 June 2016
Received in revised form 17 March 2017
Accepted 19 March 2017
Available online 31 March 2017

ABSTRACT

Soil moisture sensors are increasingly deployed in sensor networks for both agronomic research and precision agriculture. Soil-specific calibration improves the accuracy of soil water content sensors, but laboratory calibration of individual sensors is not practical for networks installed across heterogeneous settings. Using daily water content readings collected from a sensor network (42 locations × 5 depths = 210 sensors) installed at the Cook Agronomy Farm (CAF) near Pullman, Washington, we developed an automated calibration approach that can be applied to individual sensors after installation. As a first step, we converted sensor-based estimates of apparent dielectric permittivity to volumetric water content using three different calibration equations (Topp equation, CAF laboratory calibration, and the complex refractive index model, or CRIM). In a second, "re-calibration" step, we used two pedotransfer functions based upon particle size fractions and/or bulk density to estimate water content at wilting point, field capacity, and saturation at each sensor insertion point. Using an automated routine, we extracted the same three reference points, when present, from each sensor's record, and then bias-corrected and re-scaled the sensor data to match the estimated reference points. Based on validation with field-collected cores, the Topp equation provided the most accurate calibration with an *RMSE* of 0.074 $m^3\ m^{-3}$, but automated re-calibration with a local pedotransfer function outperformed any of the calibrations alone, yielding a network-wide *RMSE* of 0.055 $m^3\ m^{-3}$. The initial calibration equation used in the first step was irrelevant when the re-calibration was applied. After correcting for the reference core measurement error of 0.026 $m^3\ m^{-3}$ used for calibration and validation, the error of the sensors alone ($RMSE_{adj}$) was computed as 0.049 $m^3\ m^{-3}$. Sixty-five percent of individual sensors exhibited re-calibration errors less than or equal to the network $RMSE_{adj}$. The incorporation of soil physical information at sensor installation sites, applied retroactively via an automated routine to *in situ* soil water content sensors, substantially improved network sensor accuracy.

1. Introduction

There is growing interest in the use of sensor networks to address the "right time" dimension of precision agricultural management (Camilli et al., 2007; López Riquelme et al., 2009; Ojha et al., 2015), both through commercial applications and research on improved water-use-management (Mueller et al., 2012). Sensors that record temporally dense soil, crop or atmospheric measurements can be combined with spatial data to develop spatio-temporal models (Camilli et al., 2007; Gooley et al., 2014; Gasch et al., 2015). For agricultural sensor networks, the most commonly measured parameter is soil water content (López Riquelme et al., 2009; Greenwood et al., 2010; Coates et al., 2013; Lorite et al., 2013; Gooley et al., 2014; Goumopoulos et al., 2014).

Soil water content sensor networks can improve our understanding of vadose zone hydrologic processes at the catchment- or field-scale. Two- and three-dimensional dynamic soil water data can be used for incorporation into and validation of hydrologic and biophysical models (Frankenberger et al., 1999; Johnson et al., 2003; Stöckle et al., 2003; Mehta et al., 2004; Brooks et al.,

Abbreviations: CAF, Cook Agronomy Farm; CRIM, complex refractive index model; *RMSE*, Root Mean Squared Error; $RMSE_{adj}$, Adjusted Root Mean Squared Error; *SEL*, standard error of laboratory measurements.

* Corresponding author.
E-mail address: caley.gasch@ndsu.edu (C.K. Gasch).

http://dx.doi.org/10.1016/j.compag.2017.03.018
0168-1699/

2007), and they can directly aid in our understanding of how soil water relates to environmental properties across space and time, such as terrain (Western et al., 1999; Brocca et al., 2007), soils and tillage (Hébrard et al., 2006; Al-Mulla et al., 2009; Ibrahim and Huggins, 2011), vegetation (Korres et al., 2015), and climate (Cantón et al., 2004). Sensor networks can also facilitate soil water monitoring and inform management decisions in irrigated landscapes (O'Connell and Snyder, 2004; Salinari et al., 2014). There is great interest in developing wireless and reactive devices to ease the use of inexpensive *in situ* soil water sensors for diverse research and irrigation management applications (Cardell-Oliver et al., 2004, 2005; Akyildiz and Stuntebeck, 2006; Bogena et al., 2007; Pierce and Elliott, 2008; Ritsema et al., 2009; Korres et al., 2015), and in developing software tools for storing, screening, and delivering the vast amounts of data produced by the sensor networks (Collins et al., 2006; Illston et al., 2008; Ritsema et al., 2009; Dorigo et al., 2011).

A major challenge in obtaining network data is ensuring the sensor accuracy and precision across heterogeneous soils needed for research and management purposes (Vereecken et al., 2008). Many commercially available soil water sensors assess the relative permittivity (dielectric constant) of the bulk soil (see review by Bogena et al., 2007; Robinson et al., 2008), which is then converted to volumetric water content with a "calibration" equation—typically a quadratic function such as the Topp equation (Topp et al., 1980). Sensors may also be factory calibrated using a variety of soils and/or non-soil media (Bogena et al., 2007; Kizito et al., 2008; Decagon Devices, Inc., 2014), such that the sensors produce accurate readings in a wide range of soil types and physicochemical conditions. Using factory calibrations, manufacturers report water content accuracies of 0.01–0.03 $m^3\ m^{-3}$ in a variety of mineral and organic soils under laboratory conditions (Kizito et al., 2008; Vaz et al., 2013; Decagon Devices, Inc., 2014). However, specific characteristics of the soil at installation sites may influence the accuracy of sensor readings (Rosenbaum et al., 2010; Spelman et al., 2013; Vaz et al., 2013; Ojo et al., 2015a, 2015b), requiring sensor calibrations that account for specific soil conditions at sensor insertion sites.

The calibration of soil water content instruments can be separated into two steps: (1) the conversion of sensor electromagnetic output to apparent dielectric permittivity, and (2) the conversion of apparent dielectric permittivity to volumetric water content (Robinson, 2001). In practice, our interest in calibration accuracy primarily lies in the second step, since it is the source of most *in situ* calibration error. The conversion of apparent dielectric permittivity to volumetric water content may be customized for the specific soil of interest, or published equations can be assessed for their use and accuracy in a given soil.

The laboratory calibration approach is to measure the dielectric constant of a soil of known bulk density at different gravimetric water contents (Gardner, 1986; Young et al., 1997). Burns et al. (2014) reported a root mean squared error (*RMSE*) between 0.01 and 0.04 $m^3\ m^{-3}$ using this approach to calibrate a Stevens Hydra Probe (Stevens Water Monitoring Systems, Portland, OR) in a variety of soil textures. Spelman et al. (2013) reported errors of 0.01–0.06 $m^3\ m^{-3}$ for Decagon 10HS probes calibrated in four sandy soils using this method. Sensors can also be calibrated in the field, wherein the gravimetric water content and bulk density of field soils are used to obtain volumetric water content and regressed with sensor output. Ojo et al. (2015b) and (2015a) reported improved sensor accuracies across multiple soils using *in situ* calibration, compared with the sensor default calibrations, laboratory calibrations, and other published calibrations.

While defining soil specific calibration equations based on empirical relationships is reported to improve sensor accuracy, individual lab calibration of many sensors prior to installation is unrealistic, particularly for large sensor networks distributed across heterogeneous soils. Furthermore, if field conditions are not known or are not properly replicated in the lab, sensor performance during lab calibration may not represent performance in the field (Ojo et al., 2015b). Retroactive calibration of sensors *in situ* using the thermogravimetric method requires repeated destructive sampling, which negates the minimal disturbance benefits of using *in situ* sensors, and manipulation of soil water content in the field for sensor calibration can be difficult (Robinson, 2001). Ideally, we would like to apply a calibration method to a large number of installed sensors that accounts for site-specific soil characteristics across a heterogeneous setting.

The objective of this study was to develop an appropriate method for retroactive, sensor-specific calibration of a large number of soil water content sensors based on static, easily measured, soil physical properties (e.g. texture and bulk density). We examined variations of a two-step calibration process: (1) conversion of apparent dielectric permittivity to volumetric water content using three calibration equations, and (2) re-calibration of volumetric water content based on estimates of soil saturation, field capacity, and wilting point derived from two different pedotransfer functions.

2. Materials and methods

2.1. Site description & data collection

The R.J. Cook Agronomy Farm (CAF) is a Long-Term Agroecosystem Research site operated by Washington State University, located near Pullman, Washington, USA (Fig. 1). The farm is 37 ha in size, receives an average annual precipitation of 550 mm, primarily as winter snow and rain (Western Regional Climate Center, 2013), and is representative of dryland annual cropping systems (direct-seeded cereal grains and legume crops) of the Inland Pacific Northwest. Deep silt loam soils (Palouse, Naff, and Thatuna soil series) formed on loess hills are found at CAF, with argillic silty clay loam horizons often occurring within 1.5 m of the surface (Natural Resource Conservation Service, 2013). Long term water and tillage erosion from the steep slopes of the region have resulted in drastic redistribution of topsoil horizons and the exposure of clay rich subsoil layers, especially at soil crest positions (USDA, 1978; Kok et al., 2009; Brooks et al., 2012). The complex topography and soils of the Palouse region (including CAF) lead to variable soil profile moisture regimes influenced by watershed hydrology, microclimate, soil horizonation, cropping system, and their interactions.

To capture soil moisture variability, soil moisture sensors were installed throughout CAF from 2007 to 2009 and continue to operate today. In April 2007, we selected twelve geo-referenced locations from an existing non-aligned grid and installed ECH_2O-TE sensors (Decagon Devices, Inc., Pullman, WA) at five depths (0.3, 0.6, 0.9, 1.2, and 1.5 m) at each location. In June 2009, we installed 5TE sensors (an updated version of the ECH_2O-TE; Decagon Devices, Pullman, WA) at an additional 30 locations. At each location, we excavated a small pit to insert the 0.3 m sensor horizontally into undisturbed soil by hand; for the deeper sensors, we used an auger to create a vertical hole of appropriate depth, then inserted the sensor vertically into the undisturbed base of the hole using a hollow steel pipe modified for positioning and inserting the sensor. After placement, holes were re-filled and packed with soil. The 42 instrumented locations (a total of 210 sensors) are distributed across the research farm to represent the variety of landscape and soil conditions (see Fig. 1). Since installation, sensors have recorded volumetric water content (θ_{sensor}, $m^3\ m^{-3}$), soil temperature (°C), and bulk electrical conductivity (dS m^{-1}) hourly

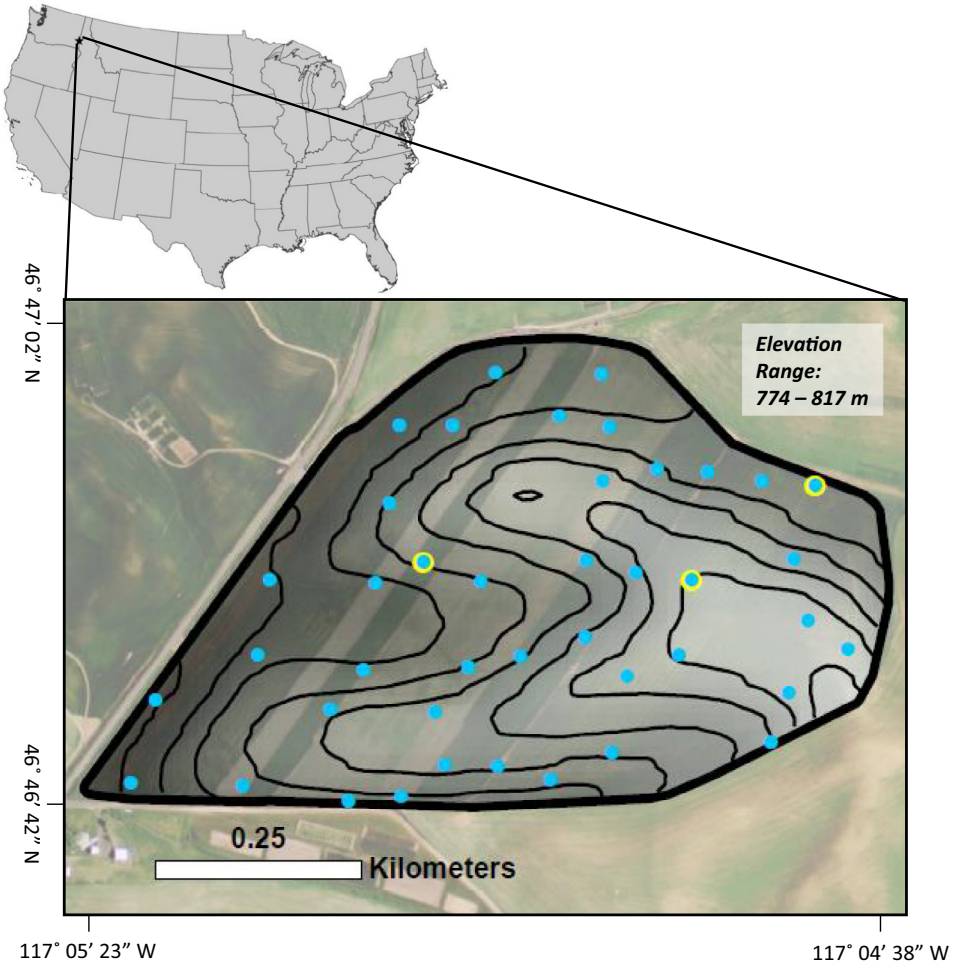

Fig. 1. Location and extent of the 37 ha Cook Agronomy Farm (CAF) Long-Term Agro-Ecosystem Research Site, near Pullman, WA, USA. Blue dots indicate the 42 locations instrumented with sensors; yellow dots indicate the three locations where replicated field cores were taken to estimate short range variability and error associated with core measurements. The map includes 5 m contours and darker shading occurs at lower elevation. (For interpretation of the references to colour in this figure legend, the reader is referred to the web version of this article.)

using EM50R radio data loggers (Decagon Devices, Pullman, WA). Data gaps occur throughout the data set, and the majority of sensors have been replaced more than once since installation, due to damage by farm equipment or sensor expiration. Thus, the sensor history at each installation site represents multiple software and hardware versions of the TE sensors. Hourly sensor data were aggregated to daily averages, and we only used daily average θ_{sensor} values from April 20, 2007 – September 19, 2014 in this analysis.

Soil physical properties throughout CAF were determined from extracted soil cores. From mid-April to mid-July 2015, known-volume soil cores at the 42 locations were extracted using a slide-hammer corer (5 cm diameter, AMS, Inc., American Falls, ID), in 10 cm increments, to 1.5 m depth (Blake and Hartge, 1986). Bulk density values calculated from these cores were used for all analyses described hereafter. Each 10 cm soil core increment was weighed, then dried 48 h in a forced air oven at 105 °C, and re-weighed to obtain bulk density (ρ_b, g cm^{-3}) and gravimetric water content (w, g g^{-1}). We calculated the volumetric water content (m^3 m^{-3}) of field-collected soils (θ_{field}) as: $\theta_{field} = w * \rho_b$. To quantify the error associated with this reference measurement, we selected three locations (see Fig. 1) at which we extracted three additional cores (early April 2014), within 1 m of one another, to 0.9 m depth, using the same coring protocol described above. From these values, we calculated the standard error of laboratory reference measurements (*SEL*) (Workman, 2001) as:

$$SEL = \left\{ \frac{\sum_{i=1}^{N} \sum_{j=1}^{r_i} (y_{ij} - \bar{y}_j)^2}{N(r_i - 1)} \right\}^{1/2}$$

where N is the number of core increments ($N = 27$), r_i is the number of replicates ($r_i = 3$), y_{ij} is the measured value of an individual core increment, and $\bar{y}_j$ is the associated mean value of the three replicated core increments. As estimated in this study, there are three primary contributing factors to *SEL*: short-range soil moisture variability (~1 m), error associated with gravimetric water content measurement; and error associated with the bulk density measurement needed to convert gravimetric to volumetric water content.

Soil particle size and additional gravimetric soil moisture measurements were determined on three other occasions, using either a hydraulic coring device (Giddings Machine Company, Windsor, CO) or hand augers. In early October 2013, we extracted soil cores (2.75 cm diameter) with a hydraulic coring device to a depth of 1.5 m at each instrumented location. We divided the top 0.9 m of each core into 10 cm sections, and also saved 10 cm sections centered around 1.2 m and 1.5 m depths. From these sections, we obtained w and calculated θ_{field} using the ρ_b values described above because cores obtained with the hydraulic coring device exhibited compaction. Six to eight sections from each core were also analyzed for particle size distribution using the pipette method (Gee and Bauder, 1986). The texture samples from the 0–0.9 m depths

did not always match sensor depths, so we fit a spline interpolation function to each particle size for each of the 42 profiles. We then predicted clay, silt, and sand content at sensor depths. On two additional occasions (early April 2013, and mid July 2014), we collected soil at each location with hand augers, retaining soil from 0.25–0.35, 0.55–0.65, 0.85–0.95, 1.15–1.25, and 1.45–1.55 m depths, and measured w. Using ρ_b measurements described previously, we computed three sets of θ_{field} values representing wet (April), intermediate (July), and dry (September) periods experienced at CAF.

2.2. Sensor calibration process

All sensor data were downloaded and archived as volumetric water content (θ_{sensor}), automatically converted from apparent dielectric permittivity (ε_a) using a factory calibration. Each sensor model has a unique factory calibration equation. Since data from our sensor network includes multiple sensor models and firmware versions (even within a single installation site), we converted all θ_{sensor} values to ε_a using equations obtained from the manufacturer, specific to each sensor's software version. From this point, we treated each installation location as a unified sensor record (hereafter 'sensor'), to which we applied a two-step calibration process (see Fig. 2).

Sensor ε_a values were converted to volumetric water content (θ_{sensor}^{*}) using three separate equations (see Table 1):

(1) θ_{Topp}: the Topp equation, a quadratic function (Topp et al., 1980);
(2) θ_{CAF_lab}: a custom calibration, a quadratic function, obtained in the lab using soil from one location at CAF according to Cobos and Chambers (2010); and
(3) θ_{CRIM}: the complex refractive index model (CRIM) (Birchak et al., 1974), which considers soil porosity, along with theoretical soil parameters (as in Rosenbaum et al., 2012).

In the second step, we re-calibrated θ_{sensor}^{*} values for each individual sensor, based on the physical properties of the soil at each installation site. We used two different pedotransfer functions (included in Table 1 and supplementary material) to obtain estimates of volumetric water content at saturation (θ_{sat}), field capacity (θ_{fc}), and wilting point (θ_{wp}) based on soil ρ_b and soil texture. Rawls and Brakensiek (1985) developed equations to estimate Brooks-Corey soil water retention parameters (Brooks and Corey, 1964) based on porosity (estimated from ρ_b), sand content, and clay content. These equations are valid for soils with sand content between 5–70% and clay content between 5–60%.

Holtan et al. (1968) provide tabular data of ρ_b and water content at multiple tensions across eight soil profiles from the Palouse region (including Palouse, Naff, and Thatuna soil series). From these data, we fit simple linear regression models between ρ_b (predictor) and water content (response) for three tension levels: −10 kPa, −30 kPa, and −1500 kPa, to provide estimates of θ_{sat}, θ_{fc}, and θ_{wp} respectively from ρ_b. This empirical data indicated a positive relationship between water content and ρ_b at all tensions up to the maximum values of ρ_b observed (1.6 g cm^{-3}). According to these relationships, volumetric water content exceeded the estimated porosity (ϕ, estimated from ρ_b, see Table 1) when ρ_b was above 1.5 g cm^{-3} at −10 kPa or above 1.58 g cm^{-3} at −30 kPa. Thus, we placed a condition on the θ_{sat} and θ_{fc} functions to constrain the water content estimates by ϕ as they approached ϕ. This modification also had the effect of reducing the available water capacity at higher ρ_b values. In summary, the Holtan-Palouse pedotransfer function combined the empirical data with conceptual

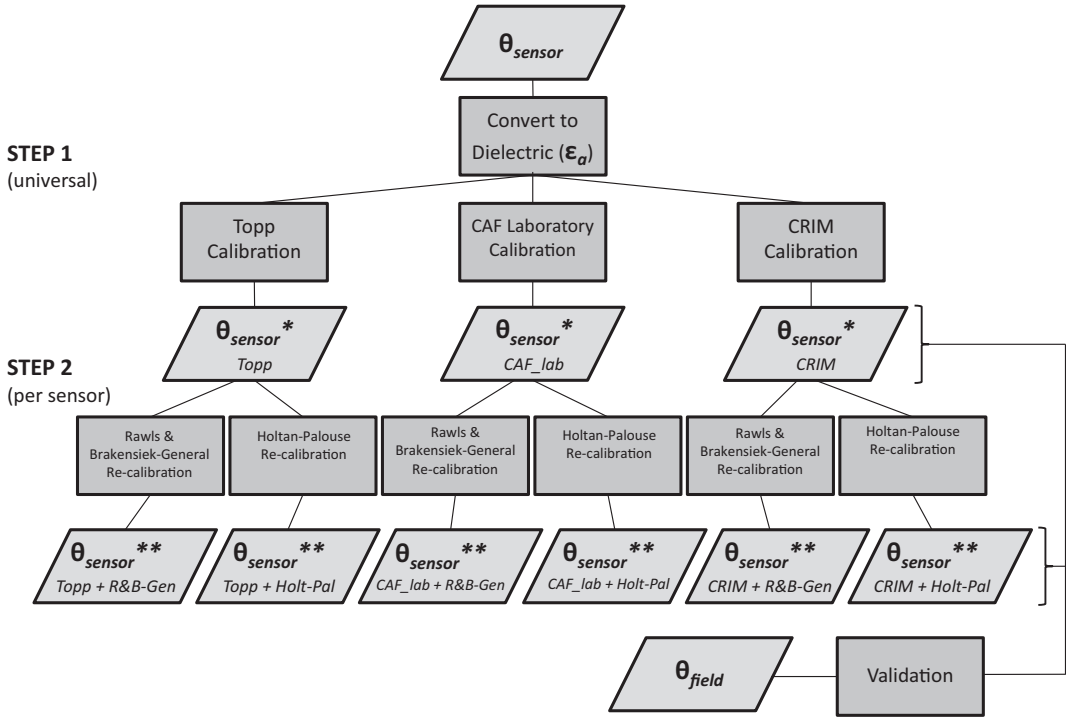

Fig. 2. Flowchart for the two-step calibration process. Prior to calibration, all sensor readings (θ_{sensor}, representing multiple sensor models and calibration equations) are converted to apparent dielectric permittivity (ε_a). The first calibration step is to convert all ε_a to volumetric water content (θ_{sensor}^{*}) using three calibration equations: Topp, CAF laboratory custom, and the complex refractive index model (CRIM). The second step is a re-calibration of individual sensors (θ_{sensor}^{**}), using estimates obtained from two pedotransfer functions: Rawls & Brakensiek-General and Holtan-Palouse. All θ_{sensor}^{*} and θ_{sensor}^{**} sets are validated with volumetric water content estimates obtained from field cores (θ_{field}).

Table 1
Calibration equations for computing θ_{sensor}^{*} from apparent dielectric permittivity (ε_a) (θ_{Topp}, θ_{CAF_lab}, and θ_{CRIM} represent respective sets of θ_{sensor}^{*}) and pedotransfer equations for estimating water content at wilting point, field capacity, and saturation, used in the re-calibration step. See supplemental material for corresponding R scripts.

Topp	$\theta_{Topp} = 0.0000043 * \varepsilon_a^3 - 0.00055 * \varepsilon_a^2 + 0.0292 * \varepsilon_a - 0.053$
CAF Laboratory	$\theta_{CAF\_Jab} = 0.0000054 * \varepsilon_a^3 - 0.00081 * \varepsilon_a^2 + 0.0447 * \varepsilon_a - 0.169$
CRIM[a]	$\theta_{CRIM} = 100 * \left(\frac{\varepsilon_a^{\beta} - (1-\phi) * \varepsilon_s^{\beta} - \phi\varepsilon_{air}^{\beta}}{\varepsilon_w(T)^{\beta} - \varepsilon_{air}^{\beta}}\right)$
Rawls & Brakensiek-General[b]	$\phi = 1 - \left(\frac{\rho_b}{2.65}\right)$
	$h_b = exp(5.34 + 0.185 * Clay - 2.484 * \phi - 0.002 * Clay^2 - 0.044*$
	$Sand * \phi - 0.617 * Clay * \phi + 0.001 * Sand^2 * \phi^2 - 0.009 * Clay^2 * \phi^2 - 0.00001*$
	$Sand^2 * Clay + 0.009 * Clay^2 * \phi - 0.0007 * Sand^2 * \phi + 0.000005 * Clay^2 * Sand$
	$+0.5 * \phi^2 * Clay)$
	$\lambda = exp(-0.784 + 0.018 * Sand - 1.062 * \phi - 0.00005 * Sand^2 - 0.003 * Clay^2$
	$+1.111 * \phi^2 - 0.031 * Sand * \phi + 0.0003 * Sand^2 * \phi^2 - 0.006 * Clay^2 * \phi^2 - 0.000002*$
	$Sand^2 * Clay + 0.008 * Clay^2 * \phi - 0.007 * \phi^2 * Clay)$
	$\theta_r = -0.018 + 0.0009 * Sand + 0.005 * Clay + 0.029 * \phi - 0.0002 * Clay^2 - 0.001*$
	$Sand * \phi - 0.0002 * Clay^2 * \phi^2 + 0.0003 * Clay^2 * \phi - 0.002 * \phi^2 * Clay$
	$\theta_{sat} = \phi - 0.1 * \phi$
	$\theta_{fc} = \left(\frac{h_b}{330}\right)^{\lambda} * (\phi - \theta_r) + \theta_r$
	$\theta_{wp} = \left(\frac{h_b}{15000}\right)^{\lambda} * (\phi - \theta_r) + \theta_r$
Holtan-Palouse	$\phi = 1 - \left(\frac{\rho_b}{2.65}\right)\theta_{sat} = ((0.0924 * \rho_b + 0.266) < (\phi - 0.1 * \phi) \rightarrow (0.0924 * \rho_b + 0.266))$
	$\wedge((0.0924 * \rho_b + 0.266) > (\phi - 0.1 * \phi) \rightarrow (\phi - 0.1 * \phi))$
	$\theta_{fc} = ((0.158 * \rho_b + 0.112) < \theta_{sat} \rightarrow (0.158 * \rho_b + 0.112)) \wedge ((0.158 * \rho_b + 0.112) > \theta_{sat} \rightarrow \theta_{sat})$
	$\theta_{wp} = 0.197 * \rho_b - 0.108$

[a] Parameters for the complex refractive index model (CRIM): β = shape factor (assumed to be 0.5), ϕ = porosity (estimated at 0.505, based on field-wide average), ε_s = solid phase dielectric permittivity (assumed to be 4.4), ε_{air} = dielectric permittivity of air (equals 1), ε_w = water dielectric permittivity (78.54 at 25 °C).

[b] Parameters for the Brooks-Corey equation (ϕ = porosity, h_b = bubbling pressure (in cm), λ = pore size distribution index, and θ_r = residual water content) are obtained, then reference points are computed for capillary pressures of 0 cm (θ_{sat}), 330 cm (θ_{fc}), and 15,000 cm (θ_{wp}). Soil particle sizes are expressed as fractions (g size class g^{-1} soil). Note that θ_{sat} is defined by Rawls and Brakensiek as the porosity (ϕ), and that the equation listed is our modification to allow for entrapped air.

modifications. While the soil profiles across the Palouse region may have changed (due to erosion) since the Holtan et al. (1968) study, the relationships between ρ_b and tension across the observed soil horizons remain valid for our purpose. Furthermore, in certain soil and crop types, it is possible that water content at field capacity and wilting point do not occur at −30 kPa and −1500 kPa respectively (Ratliff et al., 1983). It is recommended to adjust these theoretical reference points with field-based soil volumetric water content or soil water potential measurements to address this potential inaccuracy.

For both pedotransfer functions, the θ_{sat} estimate was either equivalent to, or incorporated the estimated porosity (based on ρ_b), but soils are not likely to be 100% saturated in the field, due to entrapped air. To estimate field saturation conditions, we reduced the θ_{sat} reference points provided by the pedotransfer functions by 10% of the total porosity to allow for air-filled pore spaces. The characteristics influencing the quantity of entrapped air in these soils are not known; entrapped air values reported in the literature span 1–20% of total pore volume (Constantz et al., 1988; Stonestrom and Rubin, 1989; Faybishenko 1995). Our estimate of 10% is based on entrapped air estimates in field and undisturbed soil cores that were found to be 9–13% of the total pore volume (Smith and Browning, 1943; Fayer and Hillel, 1986).

We then extracted the three reference points from each θ_{sensor}^{*} record. To extract field capacity, we developed an algorithm that recognized a sharp increase in θ_{sensor}^{*} followed by a sharp inflection and decrease in θ_{sensor}^{*} that stabilized three to ten days following the inflection point to represent a single field capacity estimate. The algorithm passed over θ_{sensor}^{*} and extracted field capacity estimates only during winter months (when living vegetation would not influence water content levels); we computed the median of all estimates to obtain a single estimate of field capacity for each sensor record (θ_{obs_fc}). According to the temperature readings of the sensors, none of the soils were frozen at sensor installation depths during the entire network history, so we do not believe that frozen conditions interfered with drainage at sensor locations. We also extracted the minimum and maximum values (θ_{min} and θ_{max}) from each θ_{sensor}^{*} record obtained under each of the three calibrations. Fig. 3 illustrates the re-calibration of a single sensor record, along with extracted and pedotransfer function estimates of the three reference points.

Depending on the number of reference points obtained from each sensor's record, we applied an appropriate function (see Fig. 4 and supplementary material) to obtain re-calibrated water content (θ_{sensor}^{**}) for each sensor. Sensors requiring re-scaling used the following function:

$$\theta_{sensor**} = \frac{Upper_{PTF} - Lower_{PTF}}{Upper_{obs} - Lower_{obs}} \times (\theta_{sensor*} - Upper_{obs}) + Upper_{PTF}$$

where $Upper_{PTF}$ and $Lower_{PTF}$ correspond to pedotransfer-derived estimates of the upper and lower reference points and $Upper_{obs}$ and $Lower_{obs}$ correspond to reference points extracted from the sensor record. When all three reference points are present, the rescaling occurs in two parts; the first part matches θ_{min} to θ_{wp} (lower) and θ_{obs_fc} to θ_{fc} (upper), the second part matches θ_{obs_fc} to θ_{fc} (lower) and θ_{max} to θ_{sat} (upper). When only two reference points are present, a single rescaling occurs between the upper and lower reference points. When only one reference point is present, a simple bias correction is applied. In total, we produced three sets of calibrated data, and six sets of re-calibrated data.

Some researchers incorporate co-measured electrical conductivity and temperature values when calibrating sensors that measure dielectric permittivity. The soils at CAF have apparent electrical conductivities below 2 dS m^{-1}. Sensors buried at the 0.3 m depth exhibit diurnal responses to temperature, but deeper sensors only exhibit annual fluctuations. In exploring correlations between the three variables, we have not observed any relationships between electrical conductivity, temperature, and volumetric water content readings. These observations are consistent with

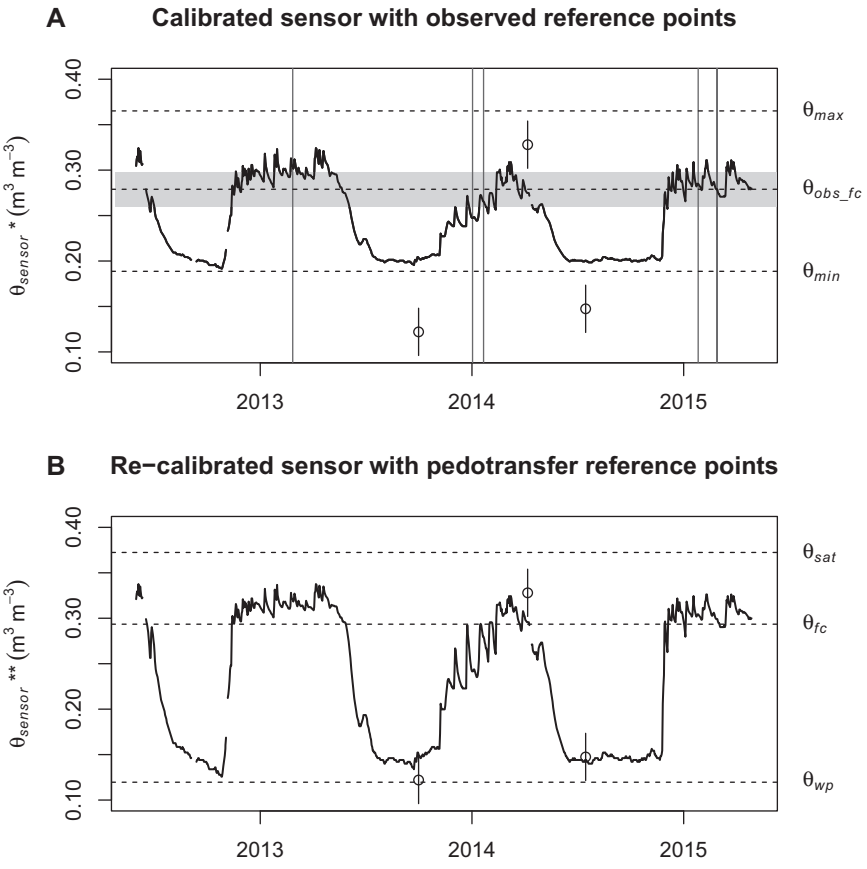

Fig. 3. (A) Illustration of water content values extracted from calibrated sensor records at the observed reference points: maximum = θ_{max} (0.407 $m^3\ m^{-3}$), minimum = θ_{min} (0.229 $m^3\ m^{-3}$), and estimated field capacity = θ_{obs_fc} (0.323 $m^3\ m^{-3}$). Vertical lines indicate dates when field capacity was automatically detected, θ_{obs_fc} is the median of the associated extracted θ_{sensor} values and the gray shaded area indicates the standard deviation of all extracted values. (B) The re-calibrated sensor record, after matching the observed reference points with those estimated by the pedotransfer functions: saturation = θ_{sat} (0.389 $m^3\ m^{-3}$), field capacity = θ_{fc} (0.322 $m^3\ m^{-3}$), and wilting point = θ_{wp} (0.155 $m^3\ m^{-3}$).

reports that the effect of conductivity on the dielectric permittivity readings is negligible in soils with apparent electrical conductivity readings below 1.7 dS m^{-1} (Visconti et al., 2014) and that temperature effects are limited to 0.02 $m^3\ m^{-3}$ for every 10 °C change in temperature (Kizito et al., 2008). For these reasons, we did not include co-measured readings of electrical conductivity and temperature in our sensor calibration approach.

2.3. Validation

To assess the performance of the calibration and re-calibration processes, we extracted $\theta_{sensor}{}^{*}$ and $\theta_{sensor}{}^{**}$ values on dates for which θ_{field} was measured. From these, we computed root mean squared error (*RMSE*) and a bias statistic:

$$RMSE = \{\frac{1}{N}\sum_{i=1}^{N}(\theta_{sensor*_i} - \theta_{field\_i})^2\}^{1/2} \quad bias = \sum_{i=1}^{N}(\frac{\theta_{sensor*_i} - \theta_{field\_i}}{N})$$

where N is the number of θ_{field} -- $\theta_{sensor}{}^{*}$ and θ_{field} -- $\theta_{sensor}{}^{**}$ pairs. We calculated these statistics for the field-wide set of θ_{field} -- $\theta_{sensor}{}^{*}$ and θ_{field} -- $\theta_{sensor}{}^{**}$ pairs (N = 517) obtained under each calibration and re-calibration. We also computed the error statistics for each individual sensor, under each calibration and re-calibration for which θ_{field}, $\theta_{sensor}{}^{*}$, and $\theta_{sensor}{}^{**}$ were available (up to three pairs per sensor).

Since the prediction error (*RMSE*) includes both the error of the sensor and the error of the reference measurement (*SEL*), and error variances are additive, we can compute the actual sensor error using the adjusted root mean squared error ($RMSE_{adj}$) as:

$$RMSE_{adj} = \sqrt{RMSE^2 - SEL^2}.$$

2.4. Software implementation

We conducted all calculations and analyses in R (R Core Team, 2015), using 'hydroGOF' (Zambrano-Bigiarini, 2014), 'lubridate' (Grolemund and Wickham, 2011), 'pastecs' (Grosjean and Ibanez, 2014), 'plyr' (Wickham, 2011), 'scales' (Wickham, 2014) and 'zoo' (Zeileis and Grothendieck, 2005) packages for data manipulation and analysis, and 'gridExtra' (Auguie, 2012), 'hexbin' (Carr et al., 2014), 'lattice' (Sarkar, 2008), and 'soiltexture' (Moeys, 2015) packages for data visualization. The supplementary material includes R code for computing reference points from pedotransfer functions, for automatically extracting field capacity estimates from sensor records, and for re-calibration (re-scaling functions and bias corrections).

3. Results

The range of soil particle sizes across the 42 locations and five depths at CAF were 42–75% silt, 12–46% clay, and 7–24% sand, with soils at sensor insertion sites falling into four soil textural classes. Bulk density ranged from 1.01 to 1.62 g cm^{-3}, and was distributed across soil textural classes (Fig. 5), but not correlated with any soil

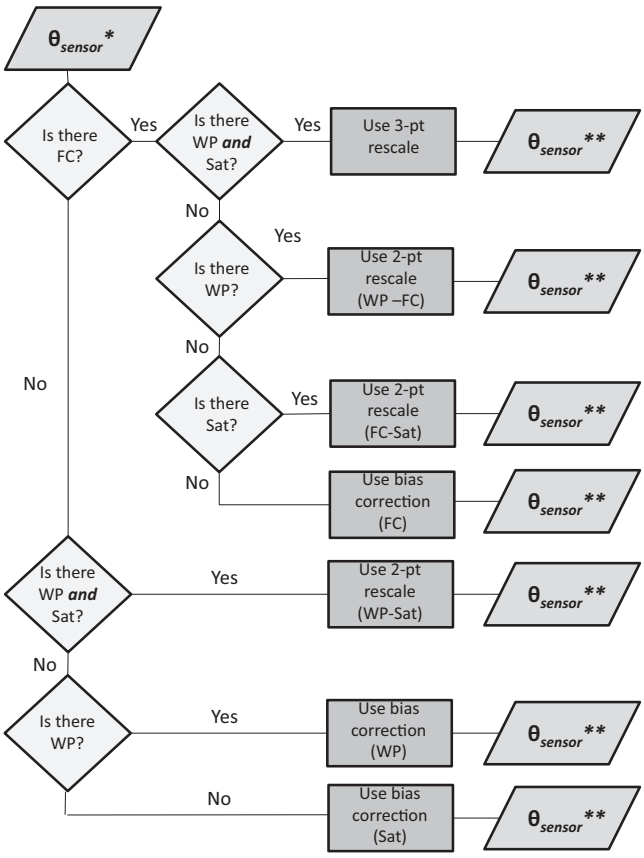

Fig. 4. Flowchart for selecting a re-calibration function based on the presence of wilting point (WP), field capacity (FC), and saturation (Sat) in sensor history. See the supplement for R code of re-calibration functions.

particle size. The estimated error (*SEL*) for θ_{field} was computed as 0.026 $m^3\ m^{-3}$, with component errors of 0.016 $g\ g^{-1}$ for gravimetric water content *w* and 0.107 $g\ cm^{-3}$ for ρ_b (both of which include short-range spatial variability).

Prior to any calibration calculation, the network-wide *RMSE* was 0.13 $m^3\ m^{-3}$, which demonstrated both scatter and bias in the factory sensor calibration (sensor readings were under-estimating water content compared to field core measurements). Of the three calibration equations that we applied to the dielectric readings, the Topp equation produced the most accurate θ_{sensor}^* values, with an *RMSE* of 0.074 $m^3\ m^{-3}$ (Fig. 6). The CAF laboratory custom calibration equation overestimated θ_{sensor}^* and produced high θ_{sensor}^* values that far exceeded the high θ_{field} values (Fig. 6). The CAF custom calibration equation produced the largest *RMSE* of all corrections. The CRIM calibration equation also overestimated θ_{sensor}^* values, particularly for high θ_{field} values (Fig. 6).

Re-calibration based on reference points obtained from the Rawls & Brakensiek-General pedotransfer function improved the accuracy of sensor readings, only when applied to the CAF laboratory and CRIM calibrations. When applied to θ_{sensor}^* values of all three calibration equations, the *RMSE* values were 0.084–0.087 $m^3\ m^{-3}$, and the bias was consistently reduced relative to that of the initial calibration (Fig. 6). In general, this re-calibration inflated θ_{sensor}^* values, particularly in ranges between field capacity and saturation, effectively under predicting low θ_{sensor}^{**} values and over predicting high θ_{sensor}^{**} values.

The re-calibration correction developed from local Palouse soils (Holtan-Palouse) produced the most accurate correction, according to validation statistics. Both the Topp and CAF laboratory custom calibrations paired with the Palouse re-calibration provided corrected sensor values with the lowest *RMSE* at 0.055 $m^3\ m^{-3}$; the Holtan-Palouse re-calibration of the θ_{sensor}^* values obtained with the CRIM calibration was only marginally worse, with an *RMSE* of 0.056 $m^3\ m^{-3}$ (Fig. 6). The hexbin plots of these corrections illustrate that the θ_{sensor}^{**} values fall on, or close to, the 1:1 line with the θ_{field} values and display minimal bias (Fig. 6). The re-calibration with the Holtan-Palouse correction provided more accurate sensor values than any of the calibration equations alone. After adjusting for the reference method error, sensor $RMSE_{adj}$ values were 0.069 and 0.049 $m^3\ m^{-3}$ for the Topp calibration and Topp calibration + Holtan-Palouse correction, respectively.

We used time-series plots of the sensor values to further visualize and qualitatively assess the different corrections. Plots of two sensors (at 0.3 and 1.5 m depths) from one location are included in Fig. 7. As mentioned, the Topp calibration provided a muted signal (particularly apparent for the sensor at 0.3 m), and it is noticeable in these plots that the re-calibration with the Rawls & Brakensiek-General pedotransfer function appeared to re-scale both sensors to the same range of values, despite differences in soil texture and bulk densities (ρ_b at 0.3 m = 1.15 $g\ cm^{-1}$ and ρ_b at 1.5 m = 1.40 $g\ cm^{-1}$). Also worth noting is that the θ_{sensor}^{**} values under either the Rawls & Brakensiek-General or Holtan-Palouse correction are very similar after re-calibration, regardless of the initial calibration equation used.

The *RMSE* values calculated for each individual sensor under the nine different calibration and re-calibration scenarios are presented as box-and-whisker plots in Fig. 8. We observed the largest range of individual sensor errors under the CAF laboratory calibration (0 to 0.332 $m^3\ m^{-3}$). Aside from one instance, the Holtan-Palouse re-calibration limited sensor error to less than

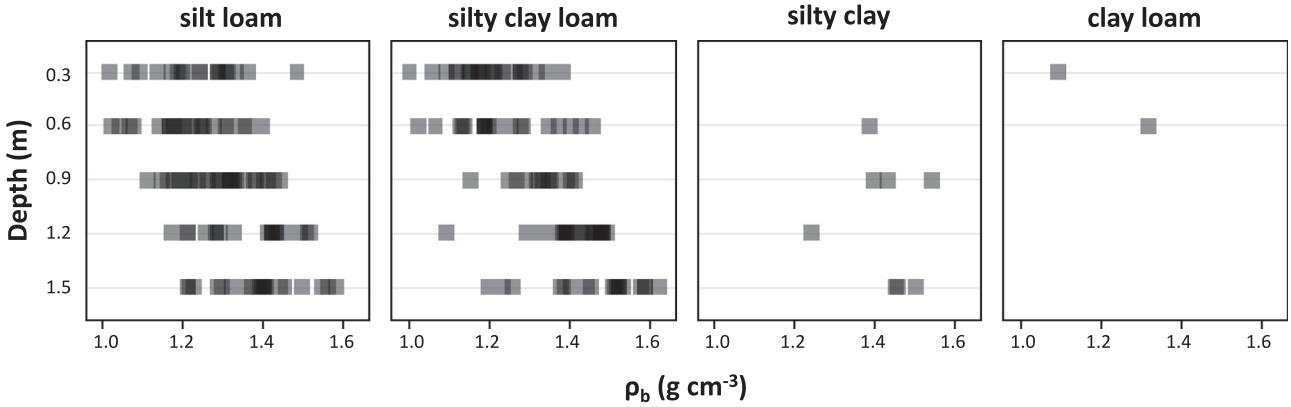

Fig. 5. Dotplots demonstrating the range of bulk density (ρ_b) values across sensor insertion sites, classified by soil textural class.

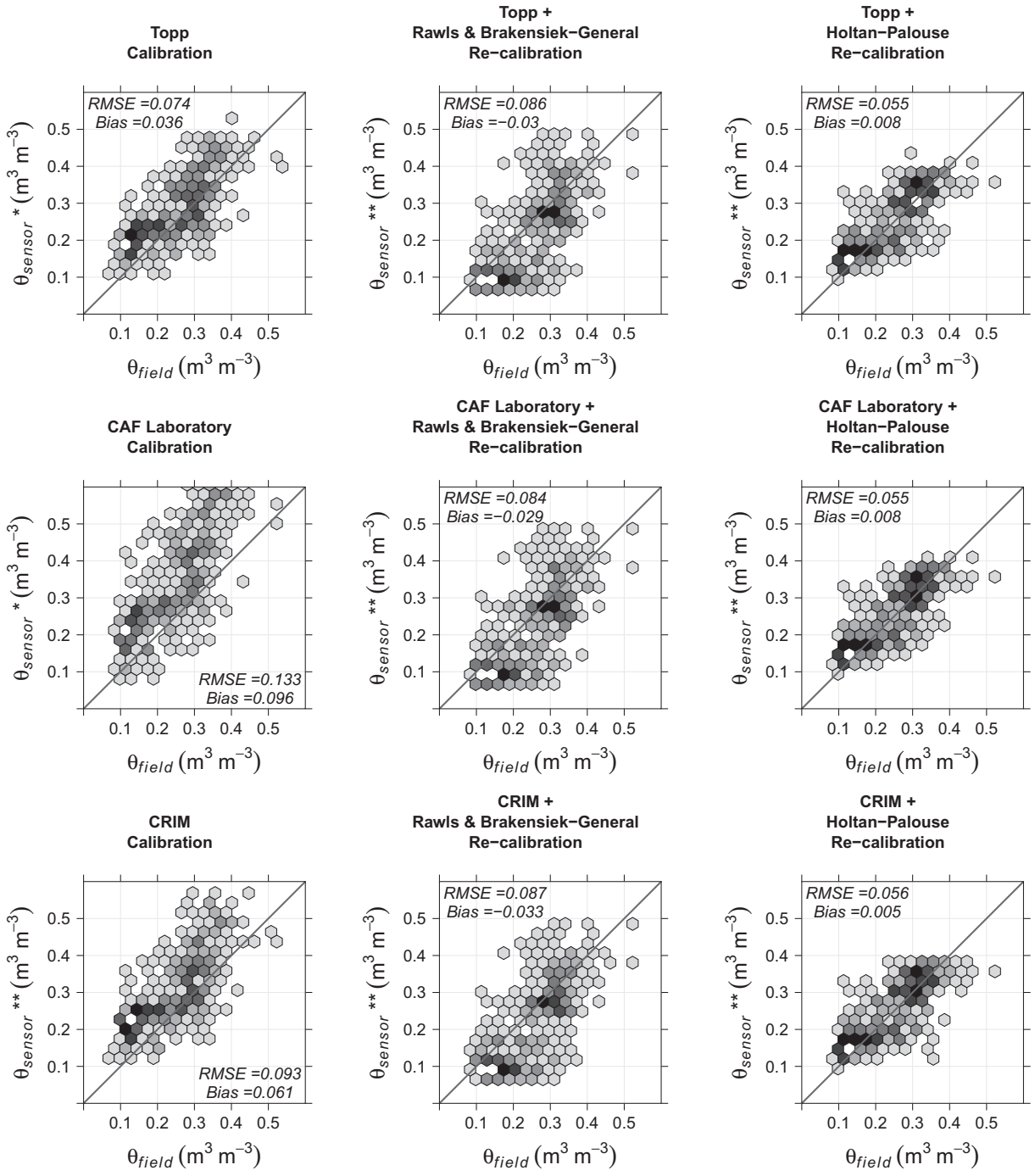

Fig. 6. Hexbin plots (binned scatterplots) of water content from field cores (θ_{field}) collected on three dates versus calibrated (θ_{sensor}^{*}) or re-calibrated (θ_{sensor}^{**}) sensor values for the same dates ($N = 517$). The network-wide *RMSE* and bias statistics are included for each comparison. Increasing shading indicates more point pairs within a hexagon bin: **Count: 1 20**. Points on the 1:1 line indicate that a θ_{sensor} value is equal to its corresponding θ_{field} value.

0.150 $m^3\ m^{-3}$, and the median *RMSE* values across the three Holtan-Palouse re-calibrations were 0.043 $m^3\ m^{-3}$.

4. Discussion

Our objective was to develop a sensor calibration approach that could be applied to a large set of sensors installed across heterogeneous soils. The methods described here achieved that by first applying a field-wide calibration equation to convert dielectric permittivity to volumetric water content, and then further correcting water content based on the physical properties of the soils at sensor insertion sites. The re-calibration step based on local soil water retention data was most important for improving the accuracy of sensor values. Under this correction, we observed an error of 0.055 $m^3\ m^{-3}$ including the reference measurement error of 0.026 $m^3\ m^{-3}$, or for sensor error alone an $RMSE_{adj}$ of 0.049 $m^3\ m^{-3}$. The manufacturer reports sensor water content accuracies of 0.01–0.03 $m^3\ m^{-3}$ for sensors calibrated using a soil-specific calibration, but such a calibration procedure would not be feasible for a large sensor network with diverse soils. High clay content and minerology can influence the dielectric and

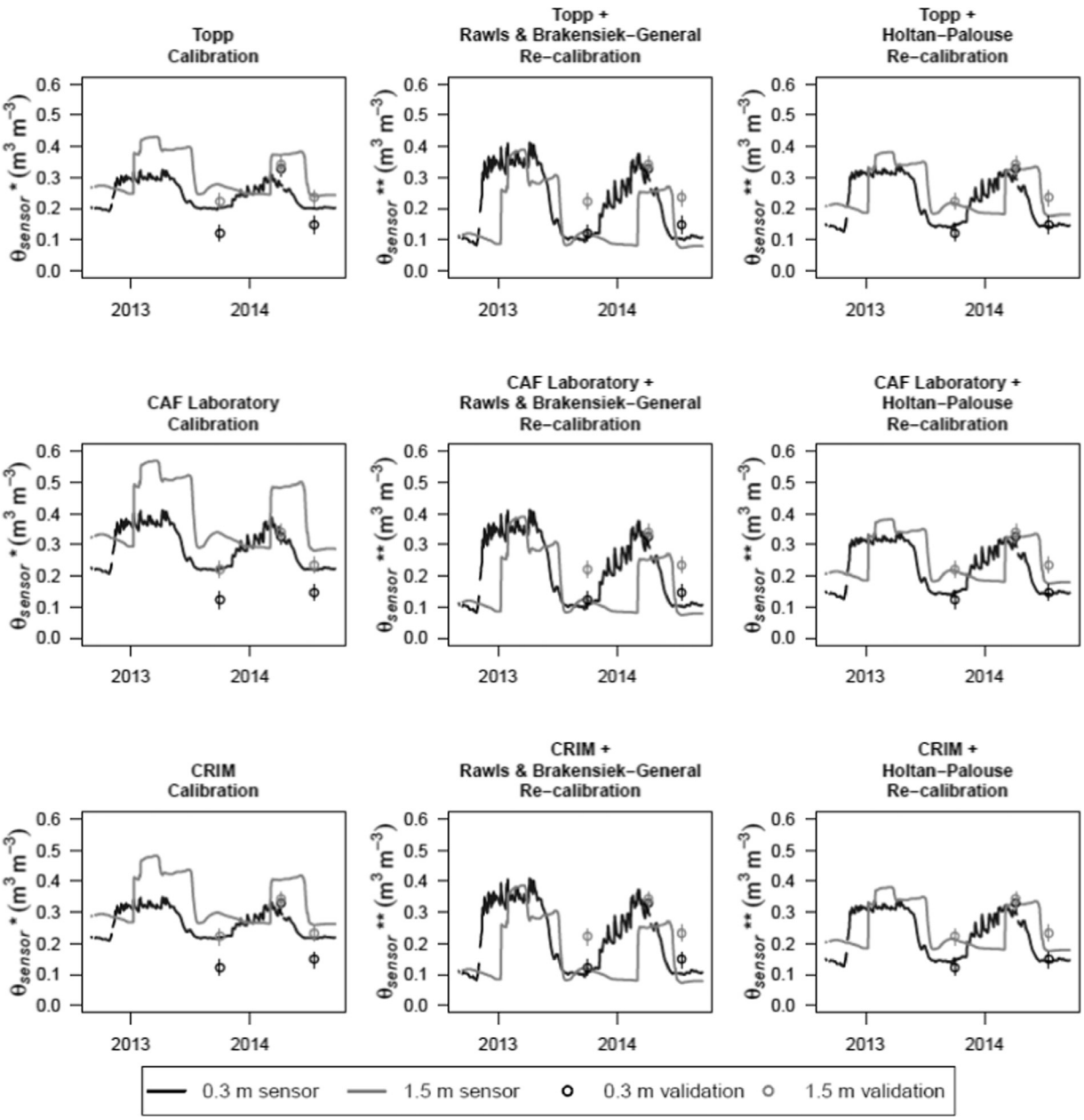

Fig. 7. Time series plots of water content values from two depths (0.3 m and 1.5 m) at one CAF location (CAF135) for a two-year period, obtained under different sensor calibrations (θ_{sensor}^{*}) and re-calibrations (θ_{sensor}^{**}). Validation points from field cores (θ_{field}) are included as hollow dots for each depth; whiskers on dots represent the precision of θ_{field} (±0.026).

conduction properties of a soil, resulting in both over- and under-estimation of water content (Stangl et al., 2009). The high clay soils monitored in this study might influence sensor calibration accuracy in this way. While these performance metrics represent what we observed for the entire network, individual sensor corrections varied in their accuracy.

In a recent publication, Cosh et al. (2016) reported volumetric soil water content *RMSE* values <0.03 $m^3\ m^{-3}$ for two commercial sensors with soil-specific calibrations. Unfortunately, the authors failed to provide a description of how the sensors were calibrated, so it is not possible to evaluate the utility and transferability of their methods. The authors also failed to describe their reference measurement methods or estimate the error of their reference method. Given that the error of our reference measurement alone was 0.026 $m^3\ m^{-3}$, we would only be able achieve *RMSE* <0.03 $m^3\ m^{-3}$ by overfitting empirical calibrations to each individual sensor – an approach of little practical utility for sensor networks.

Based on an examination of *RMSE* values calculated for each sensor and for each location (data not presented), re-calibrating using the local Holtan-Palouse pedotransfer function to estimate saturation, field capacity, and wilting point volumetric water content yielded the best results for sensors that showed clear field capacity and wilting point values in their record. Re-scaling based on saturation, when field capacity was absent, produced less accurate water content values than when field capacity was used in the re-scaling. Estimating saturation from the sensor record is difficult because the observed water content may be stabilizing at lower water content than true saturation, as defined by the pedotransfer functions. This is confounded by our lack of knowledge of entrapped air and field saturation conditions in these soils. Better methods of estimating these properties and reference points would

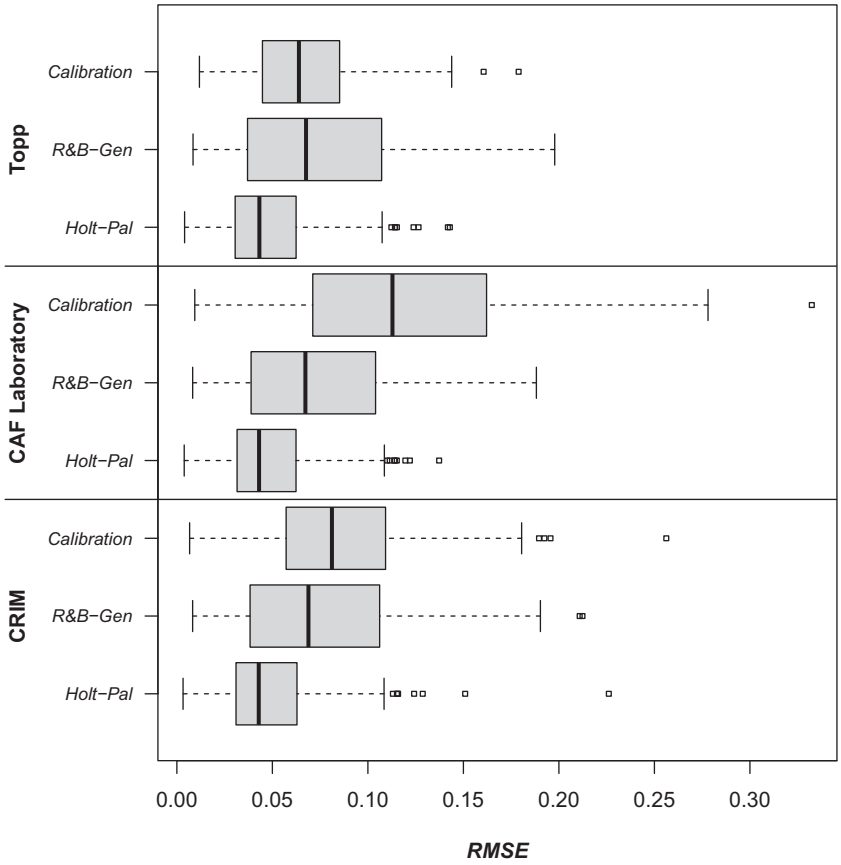

Fig. 8. Box-and-whisker plots illustrating the distribution of *RMSE* statistics for individual sensors under each calibration and re-calibration. The Rawls & Brakensiek – General re-calibration is abbreviated R&B-Gen and Holtan – Palouse re-calibration as Holt-Pal.

improve this calibration approach for soils that regularly experience saturation, or near-saturation conditions. The re-calibration also performed poorly when sensors displayed very little change through time (such that we could not determine reference points).

In addition to the uncertainty associated with identifying reference points in the sensor histories, there is opportunity to improve the re-scaling functions to more accurately reflect the relationship between tension and water content at insertion sites. For simplicity, we used linear re-scaling equations, but they could be defined by polynomial, exponential, or other non-linear equations.

We observed that the specific calibration equation used to convert dielectric permittivity to volumetric water content was fairly inconsequential to correction success when the second calibration step was applied. Currently, the Decagon 5TE sensors use the Topp calibration, which produced more accurate water content values than the CAF laboratory custom or CRIM calibrations in our soils. Thus, a custom calibration may be unnecessary when volumetric water content obtained with a factory calibration is provided by the sensor. In our case, we suspect that the CAF laboratory custom calibration was only accurate for sensors at insertion sites that were similar to the soil conditions (bulk density and mineralogy) produced in the lab. In a setting where soil physical properties are variable, such as our study site, one single custom calibration may be sub-optimal compared with a more general equation, such as the Topp equation.

The re-calibration step of this process requires soil bulk density data for sensor insertion sites, and we had the best success with a pedotransfer function developed from local soils. Any pedotransfer function could be tested for re-scaling volumetric water content, depending on the type of soil data that may be available or accessible at sensor installation locations (texture, organic matter, and bulk density). However, we observed that using a pedotransfer function developed for a wide range of soil textures did not improve sensor accuracy. The source of our local pedotransfer function, Holtan et al. (1968), includes bulk density and tension data for locations throughout the United States. This, or similar sources may serve the purpose of providing local, simple pedotransfer functions. Alternatively, tension measurements obtained from instrumented soils, laboratory measurements of retention curves, or field campaigns would provide the reference points required for the re-calibration – as well as data that could potentially be used to fit a non-linear rescaling.

A second potential limitation of this method is that it requires a sensor history long enough to provide data from which to estimate reference points (wilting point, field capacity, and/or saturation), and on which to base the re-scaling functions. Thus, it could not be used immediately for a new sensor network. If, within one growing season, or one calendar year, soil water content fluctuates enough to capture the reference points that a soil would routinely experience, this method could be applied within a year of sensor installation. As the sensor history increases, and more reference points are collected, we anticipate this calibration method to improve in accurately calibrating sensors.

5. Conclusions

The method described here provides a simple, automated, and transferable approach for retroactively correcting *in situ* soil water content sensor networks installed in diverse soils. Accurate

volumetric water content from sensors installed in sensor networks requires a second, sensor-specific correction after initial conversion to volumetric water content. The calibration process that yielded the most accurate sensor data for this network included: (1) estimating water content values at saturation, field capacity, and wilting point for each insertion site, using a local pedotransfer function, (2) identifying the same reference points in the sensor data record, and (3) re-scaling the sensor values to match the estimated retention values. This re-calibration step improved network-wide accuracy by approximately 20% compared with the first calibration step. Clearly, a sensor calibration that incorporates information about the specific soil conditions at the installation site is essential for providing accurate sensor data. While this correction is satisfactory for the CAF sensor network, it is important that this general approach is evaluated for other sensor networks, and refined for improved performance.

Acknowledgements

We wish to thank Maninder Chahal, Fidel Maureira Sotomayor, Todd Anderson, Nicole Ward, Ian Harkin, Jaimi Lambert, Ian Guest, Jack Niedbala, Yuanhong Song, David Huggins, and Chris Chambers for field, technical, and laboratory assistance. This material is based upon work that is supported by the National Institute of Food and Agriculture, U.S. Department of Agriculture, under award number 2011-67003-30341.

Appendix A. Supplementary material

Supplementary data associated with this article can be found, in the online version, at http://dx.doi.org/10.1016/j.compag.2017.03.018.

References

Akyildiz, I.F., Stuntebeck, E.P., 2006. Wireless underground sensor networks: research challenges. Ad Hoc Netw. 4 (6), 669–686. http://dx.doi.org/10.1016/j.adhoc.2006.04.003.

Al-Mulla, Y.A., Wu, J.Q., Singh, P., Flury, M., Schillinger, W.F., Huggins, D.R., Stöckle, C.O., 2009. Soil water and temperature in chemical versus reduced-tillage fallow in a Mediterranean climate. Appl. Eng. Agric. 25 (1), 45–54. http://dx.doi.org/10.13031/2013.25432.

Auguie, B., 2012. gridExtra: functions in Grid graphics. R package version 0.9.1. <http://CRAN.R-project.org/package=gridExtra>.

Birchak, J.R., Gardner, C.G., Hipp, J.E., Victor, J.M., 1974. High dielectric constant microwave probes for sensing soil moisture. Proc. IEEE 62 (1), 93–98. http://dx.doi.org/10.1109/PROC.1974.9388.

Blake, G.R., Hartge, K.H., 1986. Bulk density. In: Klute, A. (Ed.), Methods of Soil Analysis, Part 1. Physical and Mineralogical Methods. second ed. Agronomy Monograph. American Society of Agronomy, Soil Science Society of America, Madison, WI, pp. 363–375.

Bogena, H.R., Huisman, J.A., Oberdörster, C., Vereecken, H., 2007. Evaluation of a low-cost soil water content sensor for wireless network applications. J. Hydrol. 344 (1–2), 32–42. http://dx.doi.org/10.1016/j.jhydrol.2007.06.032.

Brocca, L., Morbidelli, R., Melone, F., Moramarco, T., 2007. Soil moisture spatial variability in experimental areas of central Italy. J. Hydrol. 333 (2–4), 356–373. http://dx.doi.org/10.1016/j.jhydrol.2006.09.004.

Brooks, E.S., Boll, J., McDaniel, P.A., 2007. Distributed and integrated response of a geographic information system-based hydrologic model in the eastern Palouse region. Idaho. Hydrol. Process. 21 (1), 110–122. http://dx.doi.org/10.1002/hyp.6230.

Brooks, E.S., Boll, J., McDaniel, P.A., 2012. Hydropedology in seasonally dry landscapes: The Palouse region of the Pacific Northwest, USA. In: Lin, H. (Ed.), Hydropedology: Synergistic Integration of Soil Science and Hydrology. Academic Press, Amsterdam, pp. 329–350.

Brooks, R.H., Corey, A.T., 1964. Hydraulic properties of porous media. Volume 3 of Colorado State University Hydrology Papers, 27 pages.

Burns, T.T., Adams, J.R., Berg, A.A., 2014. Laboratory calibration procedures of the Hydra Probe soil moisture sensor: infiltration wet-up vs. dry-down. Vadose Zone J. 13 (12). http://dx.doi.org/10.2136/vzj2014.07.0081.

Camilli, A., Cugnasca, C.E., Saraiva, A.M., Hirakawa, A.R., Corrêa, P.L.P., 2007. From wireless sensors to field mapping: anatomy of an application for precision agriculture. Comput. Electron. Agric. 58 (1), 25–36. http://dx.doi.org/10.1016/j.compag.2007.01.019.

Cantón, Y., Solé-Benet, A., Domingo, F., 2004. Temporal and spatial patterns of soil moisture in semiarid badlands of SE Spain. J. Hydrol. 285 (1–4), 199–214. http://dx.doi.org/10.1016/j.jhydrol.2003.08.018.

Cardell-Oliver, R., Kranz, M., Smettem, K., Mayer, K., 2005. A reactive soil moisture sensor network: design and field evaluation. Int. J. Distrib. Sens. Netw. 1 (2), 149–162. http://dx.doi.org/10.1080/15501320590966422.

Cardell-Oliver, R., Smettem, K., Kranz, M., Mayer, K., 2004. Field testing a wireless sensor network for reactive environmental monitoring [soil moisture measurement]. p. 7–12. In: Proceedings of the 2004 Intelligent Sensors, Sensor Networks and Information Processing Conference, 2004. http://dx.doi.org/10.1109/ISSNIP.2004.1417429.

Carr, D., Lewin-Koh, N., Maechler, M., Sarkar, D., 2014. hexbin: Hexagonal Binning Routines. R package version 1.27.0. <http://CRAN.R-project.org/package=hexbin>.

Coates, R.W., Delwiche, M.J., Broad, A., Holler, M., 2013. Wireless sensor network with irrigation valve control. Comput. Electron. Agric. 96, 13–22. http://dx.doi.org/10.1016/j.compag.2013.04.013.

Cobos, D.R., Chambers, C., 2010. Calibrating ECH_2O soil moisture sensors (Decagon Devices Inc. Application Note). <http://manuals.decagon.com/Application%20Notes/13393_Calibrating%20ECH2O%20Probes_Print.pdf>.

Collins, S.L., Bettencourt, L.M., Hagberg, A., Brown, R.F., Moore, D.I., Bonito, G., Delin, K.A., Jackson, S.P., Johnson, D.W., Burleigh, S.C., Woodrow, R.R., McAuley, J.M., 2006. New opportunities in ecological sensing using wireless sensor networks. Front. Ecol. Environ. 4 (8), 402–407. http://dx.doi.org/10.1890/1540-9295(2006) 4[402:NOIESU]2.0.CO;2.

Constantz, J., Herkelrath, W.N., Murphy, F., 1988. Air encapsulation during infiltration. Soil Sci. Soc. Am. J. 52 (1), 10–16. http://dx.doi.org/10.2136/sssaj1988.03615995005200010002x.

Cosh, M.H., Ochsner, T.E., McKee, L., Dong, J., Basara, J.B., Evett, S.R., Hatch, C.E., Small, E.E., Steele-Dunne, S.C., Zreda, M., Sayde, C., 2016. The Soil Moisture Active Passive Marena, Oklahoma, In Situ Sensor Testbed (SMAP-MOISST): Testbed design and evaluation of in situ sensors. Vadose Zone J. 15 (4). http://dx.doi.org/10.2136/vzj2015.09.0122.

Decagon Devices, Inc., 2014. 5TE water content, EC and temperature sensor (Decagon Devices, Inc. Product Manual). <http://manuals.decagon.com/Manuals/13509_5TE_Web.pdf>.

Dorigo, W.A., Wagner, W., Hohensinn, R., Hahn, S., Paulik, C., Xaver, A., Gruber, A., Drusch, M., Mecklenburg, S., van Oevelen, P., Robock, A., Jackson, T., 2011. The International Soil Moisture Network: a data hosting facility for global in situ soil moisture measurements. Hydrol. Earth Syst. Sci. 15 (5), 1675–1698. http://dx.doi.org/10.5194/hess-15-1675-2011.

Faybishenko, B.A., 1995. Hydraulic behavior of quasi-saturated soils in the presence of entrapped air: laboratory experiments. Water Resour. Res. 31 (10), 2421–2435. http://dx.doi.org/10.1029/95WR01654.

Fayer, M.J., Hillel, D., 1986. Air encapsulation: I. Measurement in a field soil. Soil Sci. Soc. Am. J. 50 (3), 568–572. http://dx.doi.org/10.2136/sssaj1986.03615995005000030005x.

Frankenberger, J.R., Brooks, E.S., Walter, M.T., Walter, M.F., Steenhuis, T.S., 1999. A GIS-based variable source area hydrology model. Hydrol. Process. 13, 805–822. http://dx.doi.org/10.1002/(SICI)1099-1085(19990430)1.

Gardner, W.H., 1986. Water Content. In: Klute, A. (Ed.), Methods of Soil Analysis, Part 1. Physical and Mineralogical Methods. second ed. Agronomy Monograph. American Society of Agronomy, Soil Science Society of America, Madison, WI, pp. 493–544.

Gasch, C.K., Hengl, T., Gräler, B., Meyer, H., Magney, T.S., Brown, D.J., 2015. Spatio-temporal interpolation of soil water, temperature, and electrical conductivity in 3D+T: the Cook Agronomy Farm data set. Spatial Stat. 14(part A), pp. 70–90 http://dx.doi.org/10.1016/j.spasta.2015.04.001.

Gee, G.W., Bauder, J.W., 1986. Particle-size analysis. In: Klute, A. (Ed.), Methods of Soil Analysis, Part 1. Physical and Mineralogical Methods. second ed. Agronomy Monograph. American Society of Agronomy, Soil Science Society of America, Madison, WI, pp. 383–411.

Gooley, L., Huang, J., Pagé, D., Triantafilis, J., 2014. Digital soil mapping of available water content using proximal and remotely sensed data. Soil Use Manag. 30 (1), 139–151. http://dx.doi.org/10.1111/sum.12094.

Goumopoulos, C., O'Flynn, B., Kameas, A., 2014. Automated zone-specific irrigation with wireless sensor/actuator network and adaptable decision support. Comput. Electron. Agric. 105, 20–33. http://dx.doi.org/10.1016/j.compag.2014.03.012.

Greenwood, D.J., Zhang, K., Hilton, H.W., Thompson, A.J., 2010. Opportunities for improving irrigation efficiency with quantitative models, soil water sensors and wireless technology. J. Agric. Sci. 148 (1), 1–16. http://dx.doi.org/10.1017/S0021859609990487.

Grolemund, G., Wickham, H., 2011. Dates and times made easy with lubridate. J. Stat. Softw. 40, 1–25. http://dx.doi.org/10.18637/jss.v040.i03.

Grosjean, P., Ibanez, F., 2014. pastecs: Package for Analysis of Space-Time Ecological Series R package version 1.3-18. <http://CRAN.R-project.org/package=pastecs>.

Hébrard, O., Voltz, M., Andrieux, P., Moussa, R., 2006. Spatio-temporal distribution of soil surface moisture in a heterogeneously farmed Mediterranean catchment. J. Hydrol. 329 (1–2), 110–121. http://dx.doi.org/10.1016/j.jhydrol.2006.02.012.

Holtan, H.N., England, C.B., Lawless, G.P., Schumaker, G.A., 1968. Moisture-tension data for selected soils on experimental watersheds. United States Department of Agriculture Agricultural Research Service.

Ibrahim, H.M., Huggins, D.R., 2011. Spatio-temporal patterns of soil water storage under dryland agriculture at the watershed scale. J. Hydrol. 404 (3–4), 186–197. http://dx.doi.org/10.1016/j.jhydrol.2011.04.029.

Illston, B.G., Basara, J.B., Fisher, D.K., Elliott, R., Fiebrich, C.A., Crawford, K.C., Humes, K., Hunt, E., 2008. Mesoscale monitoring of soil moisture across a statewide network. J. Atmos. Ocean. Technol. 25 (2), 167–182. http://dx.doi.org/10.1175/2007JTECHA993.1.

Johnson, M.S., Coon, W.F., Mehta, V.K., Steenhuis, T.S., Brooks, E.S., Boll, J., 2003. Application of two hydrologic models with different runoff mechanisms to a hillslope dominated watershed in the northeastern US: a comparison of HSPF and SMR. J. Hydrol. 284 (1–4), 57–76. http://dx.doi.org/10.1016/j.jhydrol.2003.07.005.

Kizito, F., Campbell, C.S., Campbell, G.S., Cobos, D.R., Teare, B.L., Carter, B., Hopmans, J.W., 2008. Frequency, electrical conductivity and temperature analysis of a low-cost capacitance soil moisture sensor. J. Hydrol. 352 (3–4), 367–378. http://dx.doi.org/10.1016/j.jhydrol.2008.01.021.

Kok, H., Papendick, R.I., Saxton, K.E., 2009. STEEP: impact of long-term conservation farming research and education in Pacific Northwest wheatlands. J. Soil Water Conserv. 64 (4), 253–264. http://dx.doi.org/10.2489/jswc.64.4.253.

Korres, W., Reichenau, T.G., Fiener, P., Koyama, C.N., Bogena, H.R., Cornelissen, T., Baatz, R., Herbst, M., Diekkrüger, B., Vereecken, H., Schneider, K., 2015. Spatio-temporal soil moisture patterns – a meta-analysis using plot to catchment scale data. J. Hydrol. 520, 326–341. http://dx.doi.org/10.1016/j.jhydrol.2014.11.042.

López Riquelme, J.A., Soto, F., Suardíaz, J., Sánchez, P., Iborra, A., Vera, J.A., 2009. Wireless sensor networks for precision horticulture in Southern Spain. Comput. Electron. Agric. 68 (1), 25–35. http://dx.doi.org/10.1016/j.compag.2009.04.006.

Lorite, I.J., Santos, C., García-Vila, M., Carmona, M.A., Fereres, E., 2013. Assessing irrigation scheme water use and farmers' performance using wireless telemetry systems. Comput. Electron. Agric. 98, 193–204. http://dx.doi.org/10.1016/j.compag.2013.08.007.

Mehta, V.K., Walter, M.T., Brooks, E.S., Steenhuis, T.S., Walter, M.F., Johnson, M., Boll, J., Thongs, D., 2004. Application of SMR to modeling watersheds in the Catskill Mountains. Environ. Model. Assess. 9 (2), 77–89. http://dx.doi.org/10.1023/B:ENMO.0000032096.13649.92.

Mueller, N.D., Gerber, J.S., Johnston, M., Ray, D.K., Ramankutty, N., Foley, J.A., 2012. Closing yield gaps through nutrient and water management. Nature 490, 254–257. http://dx.doi.org/10.1038/nature11420.

Moeys, J., 2015. soiltexture: Functions for soil texture plot, classification and transformation. R package version 1.3.3. <http://CRAN.R-project.org/package=soiltexture>.

Natural Resource Conservation Service, 2013. Whitman County, WA soil survey. <http://websoilsurvey.sc.egov.usda.gov/App/HomePage.htm>.

O'Connell, N.V., Snyder, R.L., 2004. Monitoring soil moisture with inexpensive dialectric sensors (Echoprobe) in a citrus orchard under low volume irrigation. Acta Hortic. ISHS 664 (445–451), 2004. http://dx.doi.org/10.17660/ActaHortic.664.56.

Ojha, T., Misra, S., Raghuwanshi, N.S., 2015. Wireless sensor networks for agriculture: the state-of-the-art in practice and future challenges. Comput. Electron. Agric. 118, 66–84. http://dx.doi.org/10.1016/j.compag.2015.08.011.

Ojo, E.R., Bullock, P.R., Fitzmaurice, J., 2015a. Field performance of five soil moisture instruments in heavy clay soils. Soil Sci. Soc. Am. J. 79, 20–29. http://dx.doi.org/10.2136/sssaj2014.06.0250.

Ojo, E.R., Bullock, P.R., L'Heureaux, J., Powers, J., McNairn, H., Pacheco, A., 2015b. Calibration and evaluation of a frequency domain reflectometry sensor for real-time soil moisture monitoring. Vadose Zone J. 14: 12 pages. http://dx.doi.org/10.2136/vzj2014.08.0114.

Pierce, F.J., Elliott, T.V., 2008. Regional and on-farm wireless sensor networks for agricultural systems in Eastern Washington. Comput. Electron. Agric. 61 (1), 32–43. http://dx.doi.org/10.1016/j.compag.2007.05.007.

R Core Team, 2015. R: A language and environment for statistical computing. R Foundation for Statistical Computing, Vienna, Austria. <http://www.R-project.org/>.

Ratliff, L.F., Ritchie, J.T., Cassel, D.K., 1983. Field-measured limits of soil water availability as related to laboratory-measured properties. Soil Sci. Soc. Am. J. 47, 770–775. http://dx.doi.org/10.2136/sssaj1983.03615995004700040032x.

Rawls, W.J., Brakensiek, D.L., 1985. Prediction of soil water properties for hydrologic modeling. p. 293–299. In: Proceedings of the symposium sponsored by the Committee on Watershed Management of the Irrigation and Drainage. American Society of Civil Engineering, New York, Denver CO.

Ritsema, C.J., Kuipers, H., Kleiboer, L., van den Elsen, E., Oostindie, K., Wesseling, J.G., Wolthuis, J.-W., Havinga, P., 2009. A new wireless underground network system for continuous monitoring of soil water contents. Water Resour. Res. 45 (4). http://dx.doi.org/10.1029/2008WR007071.

Robinson, D.A., 2001. Comments on "Field calibration of a capacitance water content probe in fine sand soils". Soil Sci. Soc. Am. J. 65 (5), 1570–1571. http://dx.doi.org/10.2136/sssaj2001.6551570x.

Robinson, D.A., Campbell, C.S., Hopmans, J.W., Hornbuckle, B.K., Jones, S.B., Knight, R., Ogden, F., Selker, J., Wendroth, O., 2008. Soil moisture measurement for ecological and hydrological watershed-scale observatories: a review. Vadose Zone J. 7 (1), 358–389. http://dx.doi.org/10.2136/vzj2007.0143.

Rosenbaum, U., Huisman, J.A., Weuthen, A., Vereecken, H., Bogena, H.R., 2010. Sensor-to-sensor variability of the ECH2O EC-5, TE, and 5TE sensors in dielectric liquids. Vadose Zone J. 9 (1), 181–186. http://dx.doi.org/10.2136/vzj2009.0036.

Rosenbaum, U., Bogena, H.R., Herbst, M., Huisman, J.A., Peterson, T.J., Weuthen, A., Western, A.W., Vereecken, H., 2012. Seasonal and event dynamics of spatial soil moisture patterns at the small catchment scale. Water Resour. Res. 48 (10). http://dx.doi.org/10.1029/2011WR011518.

Salinari, F., Mariani, L., Poni, S., Cola, G., Bettati, T., Diago, M.P., Tardaguila, J., Oliveira, M., 2014. Development of a water stress alert system embedded in a DSS for integrated vineyard management. Acta Hortic. ISHS 1038 (565–572), 2014. http://dx.doi.org/10.17660/ActaHortic.1038.71.

Sarkar, D., 2008. Lattice: Multivariate Data Visualization with R. Springer-Verlag, New York.

Smith, R.M., Browning, D.R., 1943. Persistent water-unsaturation of natural soil in relation to various soil and plant factors. Soil Sci. Soc. Am. J. 7(C), 114–119, http://dx.doi.org/10.2136/sssaj1943.036159950007000C0018x.

Spelman, D., Kinzli, K., Kunberger, T., 2013. Calibration of the 10HS soil moisture sensor for southwest Florida agricultural soils. J. Irrig. Drain. Eng. 139 (12), 965–971. http://dx.doi.org/10.1061/(ASCE)IR.1943-4774.0000647.

Stangl, R., Buchan, G.D., Loiskandl, W., 2009. Field use and calibration of a TDR-based probe for monitoring water content in a high-clay landslide soil in Austria. Geoderma 150 (1–2), 23–31. http://dx.doi.org/10.1016/j.geoderma.2009.01.002.

Stöckle, C.O., Donatelli, M., Nelson, R., 2003. CropSyst, a cropping systems simulation model. Eur. J. Agron. 18 (3–4), 289–307. http://dx.doi.org/10.1016/S1161-0301(02)00109-0.

Stonestrom, D.A., Rubin, J., 1989. Water content dependence of trapped air in two soils. Water Resour. Res. 25 (9), 1947–1958. http://dx.doi.org/10.1029/WR025i009p01947.

Topp, G.C., Davis, J.L., Annan, A.P., 1980. Electromagnetic determination of soil water content: measurements in coaxial transmission lines. Water Resour. Res. 16 (3), 574–582. http://dx.doi.org/10.1029/WR016i003p00574.

USDA, Soil Conservation Service, Forest Service, and Economics, Statistics, and Cooperatives Service, 1978. Palouse Co-operative River Basin Study. Washington, DC.

Vaz, C.M.P., Jones, S., Meding, M., Tuller, M., 2013. Evaluation of standard calibration functions for eight electromagnetic soil moisture sensors. Vadose Zone J. 12 (2). http://dx.doi.org/10.2136/vzj2012.0160.

Vereecken, H., Huisman, J.A., Bogena, H., Vanderborght, J., Vrugt, J.A., Hopmans, J.W., 2008. On the value of soil moisture measurements in vadose zone hydrology: a review. Water Resour. Res. 44 (4). http://dx.doi.org/10.1029/2008WR006829.

Visconti, F., de Paz, J.M., Martínez, D., Molina, M.J., 2014. Laboratory and field assessment of the capacitance sensors Decagon 10HS and 5TE for estimating the water content of irrigated soils. Ag. Water Manag. 132, 111–119. http://dx.doi.org/10.1016/j.agwat.2013.10.005.

Workman Jr., J.J., 2001. NIR spectroscopy calibration basics. In: Burns, D.A., Ciurczak, E.W. (Eds.), Handbook of Near-Infrared Analysis. Taylor & Francis, Abingdon, UK, pp. 91–128.

Western, A.W., Grayson, R.B., Blöschl, G., Willgoose, G.R., McMahon, T.A., 1999. Observed spatial organization of soil moisture and its relation to terrain indices. Water Resour. Res. 35 (3), 797–810. http://dx.doi.org/10.1029/1998WR900065.

Western Regional Climate Center, 2013. Climate Summary, Pullman, WA. <http://www.wrcc.dri.edu/>.

Wickham, H., 2011. The split-apply-combine strategy for data analysis. J. Stat. Softw. 40 (1), 1–29. http://dx.doi.org/10.18637/jss.v040.i01.

Wickham, H., 2014. Scales: Scale functions for graphics. R package version 0.2.4. <http://CRAN.R-project.org/package=scales>.

Young, M.H., Fleming, J.B., Wierenga, P.J., Warrick, A.W., 1997. Rapid laboratory calibration of time domain reflectometry using upward infiltration. Soil Sci. Soc. Am. J. 61 (3), 707–712. http://dx.doi.org/10.2136/sssaj1997.03615995006100030001x.

Zambrano-Bigiarini, M., 2014. hydroGOF: Goodness-of-fit functions for comparison of simulated and observed hydrological time series. R package version 0.3-8. <http://CRAN.R-project.org/package=hydroGOF>.

Zeileis, A., Grothendieck, G., 2005. Zoo: S3 infrastructure for regular and irregular time series. J. Stat. Softw. 14 (6), 1–27. http://dx.doi.org/10.18637/jss.v014.i06.